PHYSICAL REVIEW B VOLUME 6, NUMBER 10 15 NOVEMBER 1972

Bonding-Electron Distributions, Anharmonicity, and the Temperature Dependence of the Forbidden Si(442) Reflection*

P. Trucano† and B. W. Batterman
Department of Materials Science and Engineering, Cornell University, Ithaca, New York 14850
(Received 25 May 1972)

The forbidden Si(442) reflection was detected and its temperature dependence measured between 20 and 500 °C using Cu$K\alpha$ x-ray radiation. The reflection is extremely weak at room temperature with an integrated intensity of 4.6×10^{-11} and a structure factor $F(442)=0.035\pm 0.002$. $F(442)$ decreases to zero at 250 °C and then increases to almost twice its room-temperature value at 500 °C. This temperature dependence is consistent with contributions to the structure factor from both the antisymmetric bond charge distribution F_{bond}, and anharmonic thermal motion of the atoms F_{anh}. It was shown that F_{bond} is of opposite sign and larger in magnitude than F_{anh} at room temperature. The anharmonic contribution increases with temperature and cancels F_{bond} at about 250 °C producing zero intensity. The combination of these measurements and a recent neutron determination of F_{anh} yielded $F_{\text{bond}}=0.076\pm 0.006$ at 25 °C. This structure factor is the Fourier transform of the valence-electron distribution and like the (222) structure factor, provides a sensitive check on the accuracy of the wave functions determined from band calculations. The values of F_{bond} show a tendency to be temperature independent. However, rather large experimental errors due to the very low intensities prevented conclusions about the temperature dependence of F_{bond}.

I. INTRODUCTION

Silicon has the diamond lattice consisting of two fcc lattices, denoted A and B, and displaced $\sqrt{3}a/4$ along the unit cube diagonal where a is the unit-cell dimension. All sites have tetrahedral point symmetry and A sites are related to B sites by the inversion operation. The four nearest-neighbor atoms of each A atom lie on B sites and vice versa. Reflections with Miller indices such that $h+k+l=4n+2$ (n an integer) are the so-called forbidden reflections. When the origin is taken at an A lattice site, the structure factor F of these reflections is

$$F(h,k,l)=4f_A\langle e^{i\vec{k}\cdot\vec{u}_A}\rangle - 4f_B\langle e^{i\vec{k}\cdot\vec{u}_B}\rangle \ , \tag{1}$$

where f_A and f_B are the Fourier transforms of the charge distributions of the A and B sites and $\vec{u}_A$ and $\vec{u}_B$ are the time-dependent displacements of the charge distributions from equilibrium.

The assumptions of centrosymmetric charge distributions for A and B sites and harmonic vibrational motion implies $f_A=f_B$ and $\langle e^{i\vec{k}\cdot\vec{u}_B}\rangle=\langle e^{i\vec{k}\cdot\vec{u}_B}\rangle$. Consequently, $F(h,k,l)=0$ for the forbidden reflections, and the integrated intensity in these reflections is zero. The nonzero intensity of the forbidden (222) reflection in diamond was first measured in 1921[1] and has been measured with increasing accuracy in recent years.[2–6] The fact that this intensity is nonzero is a result of the failure of both of the above assumptions. More exact descriptions of the charge distribution and thermal motion of the silicon atoms are necessary.

The tetrahedral coordination of each silicon atom and the covalent nature of the bonding suggests the following division of the charge distribution $\rho(r)$ for each atom[7,8]:

$$\rho(\vec{r})=\rho_c(\vec{r})+\rho_a(\vec{r}) \ ,$$

where

$$\rho_c(\vec{r})=\rho_c(-\vec{r}) \quad\text{and}\quad \rho_a(\vec{r})=-\rho_a(-\vec{r}) \ .$$

$\rho_a(\vec{r})$ is antisymmetric and is the result of the buildup of charge in the bonding directions. The subscripts c and a refer to the centrosymmetric and antisymmetric charge distributions. $\rho_c(\vec{r})$ consists of a large spherical distribution due to the core electrons and eight small lobes toward and opposite to the directions of the silicon bonds. $\rho_a(\vec{r})$ consists of four positive lobes in the directions of the bonds and four negative lobes in the opposite directions. The atomic scattering factors then have real and imaginary parts $f_c(\vec{k})$ and $f_a(\vec{k})$ such that

$$f_A(\vec{k})\equiv f_c(\vec{k})-if_a(\vec{k})\equiv f_B^*(\vec{k}) \ . \tag{2}$$

$f_a(\vec{k})$ is written as the negative of the Fourier transform of ρ_a for the A atom and is expected to be a positive quantity because of the tetrahedral symmetry of the A atoms. Because f_a is about 2% of f_c at the (222) and is estimated to be less than 0.2% of f_c at the (442) reflection, Hartree–Fock calculations of the atomic scattering factors for free-silicon atoms may be used for f_c with negligible error.

The effect of thermal motion is contained in the term $\langle e^{i\vec{k}\cdot\vec{u}}\rangle$ which may be written[9]

$$\langle e^{i\vec{k}\cdot\vec{u}}\rangle \equiv e^{-\langle(\vec{k}\cdot\vec{u})^2\rangle/2}\,\langle e^{i\vec{k}\cdot\vec{u}+\langle(\vec{k}\cdot\vec{u})^2\rangle/2}\rangle \ , \tag{3}$$

where $\vec{k}=2\pi(h\vec{b}_1+k\vec{b}_2=l\vec{b}_3)$ and $\vec{u}=u_x\vec{a}_1+u_y\vec{a}_3+u_z\vec{a}_3$ in terms of the reciprocal-lattice vectors $\vec{b}_i$ and the

unit-cell vectors $\vec{a}_i$. The first term in the right-hand side (RHS) of Eq. (3) reduces to e^{-M}, where M is the Debye-Waller factor. e^{-M} is used to approximate $\langle e^{i\vec{k}\cdot\vec{u}}\rangle$ in the harmonic approximation where the crystal potential is expanded in terms of the displacements $\vec{u}$ neglecting terms higher than second order.[10] In this approximation, vibrations to $+\vec{u}$ and $-\vec{u}$ are equally likely. However, in the silicon lattice an atom sees a nearest neighbor in one direction and a "hole" in the opposite direction. If silicon atoms vibrate more toward the "holes" the motion is anharmonic, and the corrections for this type of thermal behavior are contained in the second term in the RHS of Eq. (3).

Expanding the second term in the RHS of Eq. (3) to include terms to the third order in $\vec{k}\cdot\vec{u}$,

$$\langle e^{i\vec{k}\cdot\vec{u}+\langle(\vec{k}\cdot\vec{u})^2\rangle/2}\rangle \approx 1-\tfrac{1}{6}i\langle(\vec{k}\cdot\vec{u})^3\rangle = 1-i\,8\pi^3hkl\langle u_xu_yu_z\rangle\ , \quad (4)$$

as a result of the tetrahedral symmetry of the silicon atom sites. If silicon atoms do vibrate preferentially away from their nearest neighbors, then $-\langle u_xu_yu_z\rangle_A=\langle u_xu_yu_z\rangle_B=|\langle u_xu_yu_z\rangle|$ from the A- and B-site symmetries and

$$\langle e^{i\vec{k}\cdot\vec{u}_A+\langle(\vec{k}\cdot\vec{u}_A)^2\rangle/2}\rangle \approx 1+iA(T)\ , \quad (4a)$$

$$\langle e^{i\vec{k}\cdot\vec{u}_B+\langle(\vec{k}\cdot\vec{u}_B)^2\rangle/2}\rangle \approx 1-iA(T), \quad (4b)$$

where $A(T)=8\pi^3hkl|\langle u_xu_yu_z\rangle|$. There are indications that the total charge distribution associated with each atom does not vibrate with the same amplitude.[2,11] This possibility can be partially accounted for by allowing different amplitudes of vibration for the charge described by f_c and f_a. Equations (2)–(4) may then be used to derive $F(h,k,l)$ for the forbidden reflections,

$$F(h,k,l)=-F_{\text{bond}}+F_{\text{anh}} = -8if_a\,e^{-M'}+8if_c\,e^{-M}A(T)\ , \quad (5)$$

where $M'=-\langle(\vec{k}\cdot\vec{u}_a)^2\rangle/2$. The structure factor consists of a bonding term F_{bond} due to the antisymmetric part of the atomic charge distribution and a harmonic temperature factor $e^{-M'}$. The second term of the structure factor F_{anh} contains a contribution from the more accurately known centrosymmetric part of the atomic scattering factor times the anharmonic temperature factor. The effect of the covalent charge distribution described primarily by f_a is separated from the effect of the anharmonic motion described by $A(T)$. $A(T)$ has been experimentally determined for the silicon (222) reflection using neutron diffraction.[11] $A(T)$ is proportional to the product hkl in the approximation used here. Therefore the neutron measurements can be used to estimate $A(T)$ for other forbidden reflections to the extent that the approximation $|\langle(\vec{k}\cdot\vec{u})\rangle|\ll 1$ is maintained. Temperature-dependent measurements of the silicon (222) reflection using x rays[2] have provided information concerning $f_a(222)$ and $e^{-M'}$. The measurement of the (442) reflection was undertaken to determine $f_a(442)$ which would further characterize the bonding-electron distribution, and to observe the effects of anharmonic vibrational behavior using x rays. F_{anh} is more important in temperature-dependent measurements of the (442) than in measurements of the (222) reflection because $A(T)$ is proportional to the product hkl and $f_a(442)$ is expected to be smaller than $f_a(222)$.

The integrated intensity of the (442) reflection has been estimated to be about three orders of magnitude less than the (222) reflection which is already a relatively weak reflection. Success in measuring these intensities depends, in a large part, on the use of modern detection equipment and careful use of several diffraction effects to maximize signal-to-noise ratios and aid in aligning crystals.

II. EXPERIMENTAL

A double crystal spectrometer in the $(m, -n)$ mode provided maximum signal-to-background ratios. A Si(440) reflection from the first crystal resulted in a good match of d spacings and a strong incident beam. This mismatch in planar spacings resulted in a Cu $K\alpha_1-K\alpha_2$ separation of 143″ of arc in the (442) reflection. Vertical divergence of 1.3° was allowed. Both crystals were oriented and cut on a diamond saw. Each was ground on succeedingly finer grades of SiC powder in water to 800 grit and etched for 4 min in CP-4[12] to remove strains and damaged surface layers. To orient the (442) planes parallel to the crystal's surface the (884) reflection and Mo $K\alpha$ radiation were used.

To obtain the minimum width in the (442) reflection, the diffraction vectors of the first and second crystals must be in the same plane. This was accomplished by orienting a second low-dislocation crystal cut with the (440) planes parallel to the surface and placing it in the second crystal's position. The diffraction vector of the second crystal was perpendicular to the axis of rotation of the second crystal. Then the (440) reflection was found and the tilt of the first adjusted until the theoretical width was obtained. To achieve minimum width in the (442) reflection one needed only to ensure that the (442) planes were oriented perpendicular to the axis of its barrel holder before being placed in the spectrometer.

The second crystal was mounted in the furnace shown schematically in Fig. 1. The crystal was held in a copper block with two chromel-alumel thermocouples attached to the edges of the crystal and insulated from the block. A Be heat shield was positioned in front of the crystal and attached to the copper block. The block was heated by

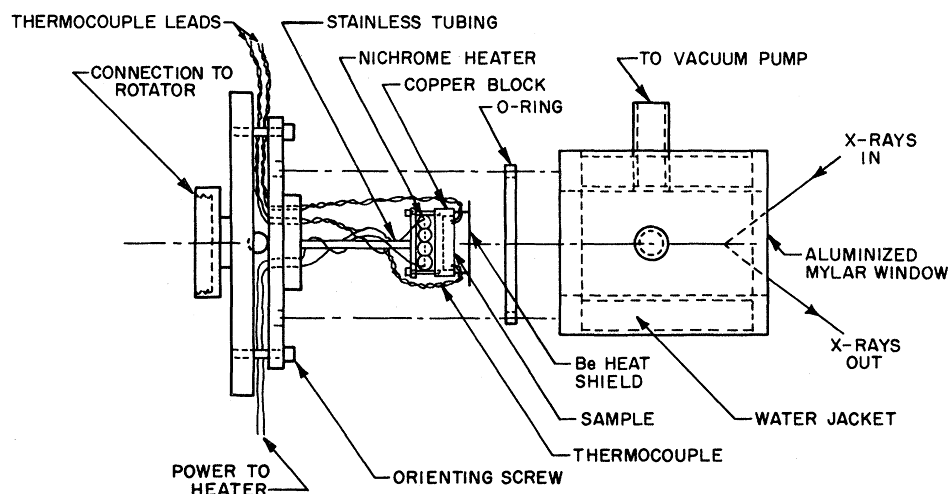

FIG. 1. Furnace schematic.

nichrome wire and insulated from the base by a length of stainless-steel tubing. The furnace was water cooled and evacuated. A 0.002-in. Mylar window with a 100-Å-thick vapor-deposited Al film to increase thermal reflectance allowed x rays into and out of the furnace. Heater current was proportionally controlled to within 1 °C and the two thermocouples read within 5 °C of each other at all temperatures.

The base of the furnace was adjustable via four screws which tilted the furnace with respect to its barrel mount. The crystal could be oriented via the (884) reflection after it was placed in the furnace and before the barrel mount was positioned in the spectrometer. The whole furnace could be rotated about the (442) diffraction vector (denoted a ϕ rotation) by the rotation of a shaft on preloaded bearings in the barrel mount. The ϕ rotation could be performed with the crystal's θ position maintained to within 150″ of arc.

Noise levels and harmonic contaminants in the diffracted beam were minimized by the use of a lithium-drifted silicon solid-state detector. The energy resolution of ~300 eV allowed electronic discrimination of the various energy components in the diffracted beam and resulted in an electronic noise level of 0.004 counts/sec. A Coolidge copper x-ray tube and generator with line stabilizer was run at 45 kV and 15 mA for all measurements.

Because the (442) reflection is extremely weak, its θ position must be located precisely before attempting to measure the intensity. The absence of long-wavelength harmonics in the diffracted beam complicated this problem. Short-wavelength harmonics were present but were too weak to be helpful in locating the reflection. The problem was solved by locating a set of (440) planes in the second crystal which made a relatively low angle with the (442) planes. The asymmetric reflection from these (440) planes was easily found at the appropriate θ and ϕ angles. The angular θ distance from the (440) reflection to the (442) reflection was calculated and the second crystal was rotated using a micrometer drive. This technique located θ_{442} to within 150″ of arc.

This θ position was not accurate enough to locate the (442) position but readily produced one of the stronger Umweganregung reflections[13,14] upon scanning in the ϕ direction. Once an Unweganregung peak was found, θ was tuned to maximize this intensity. This θ setting located the (442) peak position precisely and Umweganregung plots could be obtained for Cu$K\alpha_1$ or Cu$K\alpha_2$ depending on which wavelength was set to diffract. Figure 2 shows a ϕ plot for Cu$K\alpha_1$ radiation along with the calculated positions of the multiple-scattering events. The calculated positions were obtained using a computer program following Cole *et al.*[14] The (442) ϕ plot repeats every 180° and contains a mirror reflection about $\phi = 0°$. The Umweganregung peaks allowed accurate positioning of the counter and its receiving slit. Because the 2θ position of the multiply diffracted beam is exactly the same as the (442) diffracted beam, the Umweganregung peaks from Cu$K\alpha_1$ and Cu$K\alpha_2$ radiation indicated the spacial positions of the (442) $K\alpha_1$ and $K\alpha_2$ diffracted beams. With the extremely low counting rates [0.4 counts/sec at the (442) $K\alpha_1$ peak and 0.2-counts/sec background], it is doubtful that the receiving slits or counter could have been positioned accurately enough to make the measurements without the aid of the Umweganregung reflections.

All θ scans were made at ϕ positions of 8°, 44°, 136°, 172°, 188°, 224°, 316°, and 352°, three of which are shown in Fig. 2. A Cu$K\alpha$ Umweganregung peak adjoining the desired region was found. The peak θ position was noted and the receiving

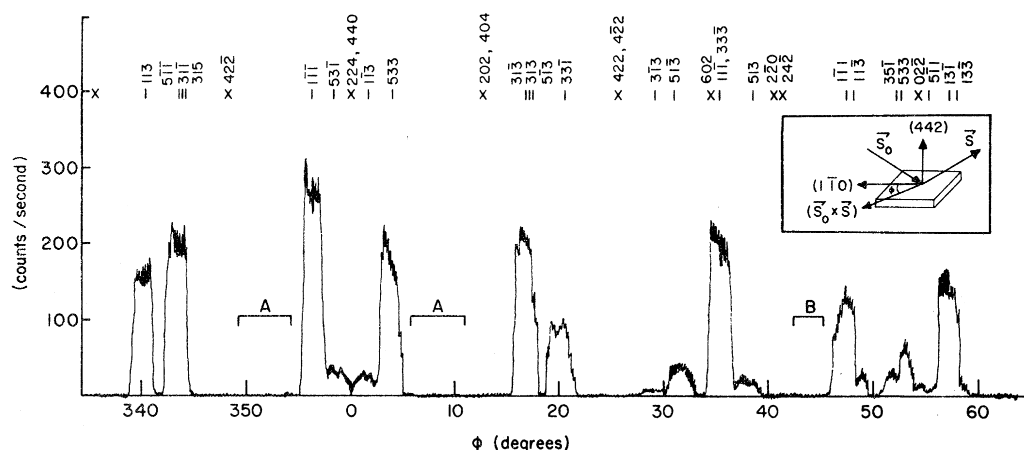

FIG. 2. Si(442) Umweganregung pattern: Intensity in the (442) diffraction direction as the crystal was rotated about the (442) diffraction vector. The orientation of the crystal with the incident beam direction $\vec{s}_0$ and the diffracted beam direction $\vec{s}$ is shown in the inset. *A*- and *B*-type Umweganregung free regions used in the (442) intensity measurements are indicated. The plot repeats every 180° in ϕ and inverts through $\phi = 0°$. The calculated positions of Umweganregung and Aufhellung regions are indicated above the plot by slashes and crosses, respectively.

slit, counter, and antiscattering shields adjusted. The crystal was rotated into the Umweganregung free region by the appropriate ϕ rotation, and θ was set off the peak. θ scans through the (442) peak were made in 22 h, scanning at a rate of 0.8″ of arc/min. A digital printer recorded the counts accumulated every 10 min. The resulting data for a room-temperature run are plotted in Fig. 3. Integrated intensities were obtained by subtracting the average background level from the total number of counts in a region three times the $K\alpha_1$-$K\alpha_2$ separation. Scans were repeated many times to obtain the desired statistical accuracy.

Before and after each θ scan, the incident beam intensity was monitored by measuring the scattering from a piece of polystyrene placed in the incident beam at a fixed position. The incident beam intensity varied slowly with a period of one day or more. The intensity changed less than 3% during any θ scan and varied less than 6% during the course of the experiment. The absolute incident beam was obtained by comparing the polystyrene scattering to the diffracted power from the silicon (222) reflection. A crystal with the (222) planes parallel to the surface was prepared in the same manner as the (442) and (440) crystals. Umweganregung plots were calculated and obtained experimentally. Many θ scans were made at four different ϕ positions chosen to eliminate the effects of Umweganregung and Aufhellung intensities. θ scans through the (222) peak were made in 16.7-min scanning at a rate of 72″ of arc/minute. Peak intensities of 180 counts/sec and the expected $K\alpha_1$-$K\alpha_2$ separation of about 400″ of arc were observed. The (222) diffracted power was obtained by subtracting the total counts in a region three times the (222) $K\alpha_1$-$K\alpha_2$ separation. The integrated intensity for the Si(222) reflection was calculated using the kinematic formula and a structure factor 1.46 ± 0.04 as determined by Roberto and Batterman.[2] Although low-dislocation crystals were used in this experiment, the dynamical and kinematic theories predict values differing by less than 2% for the (222) integrated intensity. The mea-

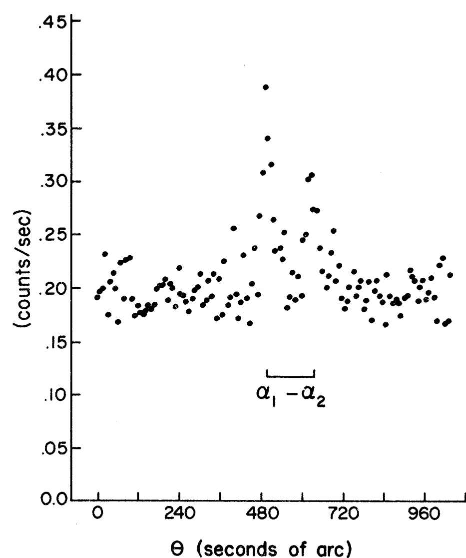

FIG. 3. Room-temperature Si(442) θ scan: Diffracted intensity is plotted vs θ angle. Scan was made at 0.8″ of arc/min and each point represents 10 min of counting time. Clearly separated $K\alpha_1$ and $K\alpha_2$ peaks are shown with the calculated $K\alpha_1$-$K\alpha_2$ separation.

surement of the diffracted power from the (222) reflection determined that the incident intensity was $(1.16\pm0.10)\times10^{6}$ counts/second which was corrected after each run for variations in the polystyrene monitor.

III. RESULTS

From each of the Umweganregung free regions, A and B, indicated in Fig. 2, three other equivalent regions may be obtained from the symmetry of the (442) ϕ plot. Several room-temperature measurements of the (442) integrated intensity were made at all eight ϕ positions. The intensities from the four B-type regions at $\phi=44°$, 136°, 224°, and 316° were consistently higher than the intensities in the A-type regions by about 65%. Furthermore, as ϕ was varied around 316°, the intensity measured in the θ scans increased. It was concluded that scattering from the tails of the (531) Umweganregung peak or air scattering from radiation diffracted into other directions at the $(2\bar{2}0)$ Aufhellung region affected the measured intensities. No such variation in the intensities of the θ scans was observed as ϕ was varied within the A regions.

Nine room-temperature θ scans in the A regions were used to calculate the integrated intensity of the (442) reflection. Typical θ scans (see Fig. 3) showed well-resolved Cu$K\alpha_1$ and Cu$K\alpha_2$ peaks with the expected angular separation. Analysis of several runs showed the intensity in the $K\alpha_1$ peak is twice that in the $K\alpha_2$ peak. The data from the nine θ scans are summarized in Table I, and combined to give a room-temperature integrated intensity of

$$(E\omega/I_0)^{\mathrm{RT}}_{442}=(4.6\pm0.6)\times10^{-11}\ .$$

Using the kinematic equation for the integrated intensity, the structure factor for the (442) reflection is calculated to be

$$|F(442)|=0.035\pm0.002\ .$$

The kinematic and dynamic calculations of integrated intensities using structure factors of this magnitude differ by less than 0.2%. An absorption constant of $\mu=144\ \mathrm{cm}^{-1}$ [15] and Debye temperature of 543 °K[16] were used in the calculation and the polarization factor was computed using a Darwin–Prins computer calculation of the reflectances from the (440) first crystal.

Neutron measurements of the Si(222) intensity[11] were used to calculate $F_{\mathrm{anh}}(442)$. Keating *et al.*[11] expressed the anharmonic parameter $A(T)$ as

$$A(T)=(2\pi/a\alpha)^3\beta hkl\,(k_B T)^2, \qquad (6)$$

where $\alpha=7.85\times10^{-12}$ erg Å^{-2} and β is a parameter obtained from the experimentally determined neutron (222) integrated intensity. At room temperature $\beta=(5.53\pm0.55)\times10^{-12}$ erg Å^{-3}. Evaluating $A(T)$ from Eq. (6) and solving for F_{bond} in Eq. (5) we find

$$|F_{\mathrm{bond}}|=0.007\pm0.006 \text{ or } 0.076\pm0.006.$$

$f_c=f+\Delta f'+i\Delta f''$ was taken as $f=5.85$,[17] $\Delta f'=0.24$,[18] and $\Delta f''$ was calculated from the absorption constant. The two values represent the possibilities of having a bonding term larger or smaller than the anharmonic term. To discriminate between these two values the temperature dependence of $F(442)$ was measured. The neutron measurements[11] show that the anharmonic term increases approximately with the square of the temperature and the electronic contribution was expected to decrease rather slowly.

Temperature-dependent measurements were made at one azimuth, $\phi=8°$, and at temperatures from 22 to 505 °C. The procedures were identical with the room-temperature measurements, and the results are summarized graphically in Fig. 4. Because the intensity decreased, went through a minimum, and then began to increase, the bonding term must have been of greater magnitude at room temperature and of the opposite sign from the anharmonic term.

The anharmonic contribution to $F(442)$ was calculated at each temperature from the neutron measurements of β.[11] Table II summarizes the data including the values of β and both roots resulting from the quadratic equation. Root 1 is correct if $|F_{\mathrm{bond}}|>|F_{\mathrm{anh}}|$ and root 2 is correct if $|F_{\mathrm{bond}}|<|F_{\mathrm{anh}}|$. These two values of F_{bond} are plotted in Fig. 5. Below 250 °C the larger root is correct and above 250 °C the smaller root is applicable. The intersection of the lines formed by the two roots indicates the temperature where $|F_{\mathrm{bond}}|=|F_{\mathrm{anh}}|$. Included in Fig. 5 are lines indicating the expected temperature dependence of the bonding contribution to $F(442)$ if the charge represented by f_a vibrates with the same mean-square amplitude as the centrosymmetric charge distribution or with half that mean-square amplitude.

IV. DISCUSSION AND CONCLUSIONS

One of the more important aspects of the work described here is the description of the techniques

TABLE I. Room-temperature integrated intensities for Si(442) reflection measured at A-type Umweganregung free regions indicated in Fig. 2. Statistical error in x-ray count for all numbers is $\pm1.9\times10^{-11}$. Average of A-type measurements: $(4.6\pm0.6)\times10^{-11}$.

$\phi=8°$ (10^{-11})	$\phi=172°$ (10^{-11})	$\phi=188°$ (10^{-11})	$\phi=352°$ (10^{-11})
5.28	3.72	4.70	5.22
4.66	3.78	4.45	4.71
4.53			

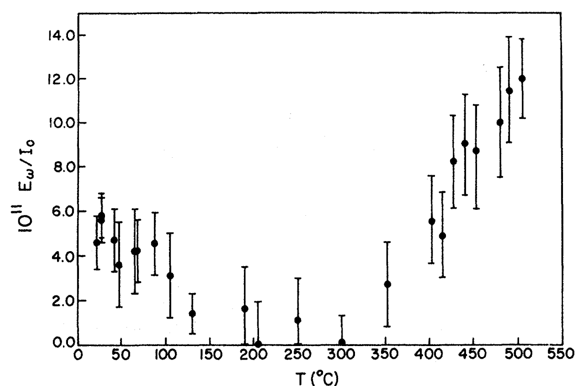

FIG. 4. Si(442) integrated intensity vs temperature: (442) integrated intensity is shown decreasing to a minimum at 250 °C and then increasing. For a discussion of the errors, see the text.

used to measure the extremely weak intensity of the Si(442) reflection with x rays. Previous measurements of the Si(222) integrated intensity, which is 100 times smaller than allowed reflections, were difficult but rather straightforward. Measurement of the (442) reflection, which is 1000 times smaller than the (222), is extremely difficult. In contrast to most integrated intensity measurements where a reflection is found by very coarse alignment, and then finer adjustments are made before the measurement, the (442) reflection had to be located and the crystals aligned to maximum precision before the time-consuming measurement procedure was begun. The experiment was designed to provide a capability for measuring weak x-ray integrated intensities which has not been realized previously.

Room-temperature measurements of the (442) integrated intensity yielded two possible values for the electronic contribution to $F(442)$. Definite experimental numbers were only obtained from a combination of the room-temperature measurement and the qualitative temperature dependence of the (442) integrated intensity. From the two sets of data summarized in Table I and Fig. 4, several conclusions may be drawn.

(i) The temperature dependence of the (442) reflection determined the room-temperature value of the bonding electron contribution to the structure factor as

$$|F_{\text{bond}}| = 0.076 \pm 0.006 .$$

All other possible values for the electronic contribution to $F(442)$ derived from the room temperature measurement are inconsistent with the observed temperature dependence. This value is relevant to two areas of research. Silicon structure factors have been analyzed to determine the departures from spherical atomic-charge distributions.[19,20] Dawson and Sanger[19] have reviewed the work in this area and predicted a value for the (442) electronic-scattering factor:

$$|F_{\text{bond}}(442)| = 0.064 ,$$

where the Debye–Waller factors of the core and bonding electrons were assumed to be the same. This value is in good agreement with our measured (442) electronic-scattering factor. The second area of study relevant to these measurements con-

TABLE II. Partial listing of temperature dependent Si(442) data and calculated contributions to the structure factor.

T (°K)	$E\omega/I_0$ (10^{-13})	$\lvert F \rvert$	β (10^{-12} erg Å^{-3})	$\lvert F_{\text{anh}} \rvert$	$\lvert F_{\text{bond}} \rvert_1$	$\lvert F_{\text{bond}} \rvert_2$
295	463 ± 120	$0.035^{+0.004}_{-0.005}$	5.53	0.040 ± 0.004	$0.075^{+0.009}_{-0.009}$	$0.005^{+0.009}_{-0.008}$
320	359 ± 190	$0.031^{+0.007}_{-0.010}$	5.40	0.046 ± 0.004	$0.077^{+0.011}_{-0.014}$	$0.015^{+0.014}_{-0.010}$
341	420 ± 140	$0.033^{+0.006}_{-0.006}$	5.30	0.051 ± 0.004	$0.084^{+0.009}_{-0.010}$	$0.017^{+0.011}_{-0.009}$
379	313 ± 190	$0.029^{+0.008}_{-0.011}$	5.11	0.059 ± 0.004	$0.088^{+0.012}_{-0.015}$	$0.031^{+0.015}_{-0.012}$
402	141 ± 90	$0.019^{+0.006}_{-0.007}$	5.00	0.065 ± 0.004	$0.084^{+0.009}_{-0.012}$	$0.046^{+0.012}_{-0.010}$
477	0 ± 190	$0.000^{+0.023}_{-0.000}$	4.70	0.083 ± 0.004	$0.085^{+0.024}_{-0.004}$	$0.081^{+0.004}_{-0.024}$
573	8 ± 120	$0.005^{+0.014}_{-0.005}$	4.31	0.106 ± 0.003	$0.107^{+0.019}_{-0.003}$	$0.104^{+0.003}_{-0.019}$
626	273 ± 190	$0.027^{+0.008}_{-0.012}$	4.09	0.117 ± 0.003	$0.143^{+0.012}_{-0.016}$	$0.091^{+0.015}_{-0.012}$
676	555 ± 190	$0.039^{+0.006}_{-0.008}$	3.89	0.127 ± 0.003	$0.165^{+0.009}_{-0.010}$	$0.089^{+0.010}_{-0.009}$
701	821 ± 210	$0.047^{+0.006}_{-0.006}$	3.80	0.132 ± 0.003	$0.178^{+0.009}_{-0.009}$	$0.086^{+0.009}_{-0.009}$
726	868 ± 210	$0.048^{+0.006}_{-0.006}$	3.73	0.137 ± 0.003	$0.185^{+0.009}_{-0.009}$	$0.090^{+0.009}_{-0.009}$
752	999 ± 250	$0.052^{+0.006}_{-0.007}$	3.64	0.142 ± 0.003	$0.194^{+0.009}_{-0.010}$	$0.091^{+0.010}_{-0.009}$
778	1197 ± 180	$0.057^{+0.004}_{-0.005}$	3.57	0.148 ± 0.002	$0.204^{+0.006}_{-0.006}$	$0.092^{+0.006}_{-0.007}$

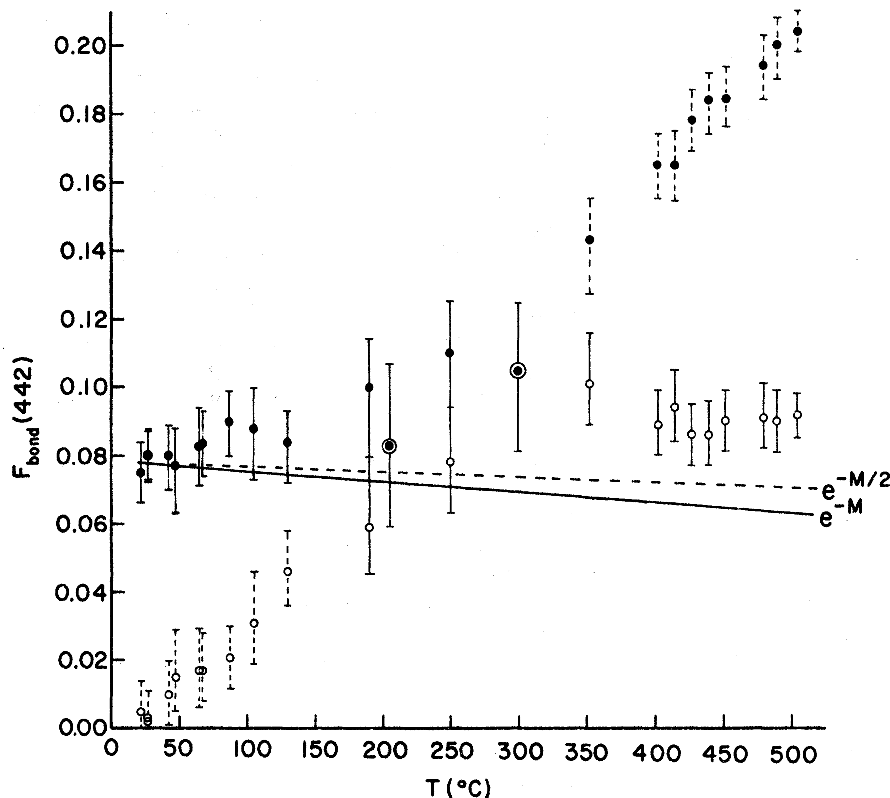

FIG. 5. $F_{bond}(442)$ vs temperature: Both roots resulting from the solution of Eq. (5) for F_{bond} are plotted. The intersection of the lines formed by the two roots indicates the temperature at which the anharmonic contribution to $F(442)$ is canceled by the bonding contribution. If $|F_{bond}| > |F_{anh}|$, the larger root (indicated by solid circles) is correct, and if $|F_{bond}| < |F_{anh}|$, the smaller root (indicated by open circles) is correct. The solid and dashed lines indicate the expected temperature dependence of $F_{bond}(442)$ if the antisymmetric charge vibrates with the same or with half the mean-square amplitude of the core electrons.

cerns band calculations for silicon. These calculations include considerations of the localization of the bonding-electron distribution and the amount of charge in the bond.[21,22] The Si(222) scattering factor has provided a sensitive check on these calculations and the (442) scattering factor presents new bases for comparison.

(ii) The temperature dependence of the (442) reflection confirms the existence of anharmonic thermal vibrations in silicon. Experimental evidence of these effects was obtained only recently by a neutron-diffraction experiment.[11]

(iii) The qualitative (442) temperature dependence is direct evidence that the bonding contribution to the structure factor of forbidden reflections is of opposite sign to the contribution from anharmonic vibrations. If the two terms had the same sign the (442) intensity could only increase with temperature. This result is expected if one assumes the atoms vibrate preferentially away from their nearest neighbors.

Before any conclusions are drawn from quantitative temperature-dependent results shown graphically in Fig. 5, the errors and approximations used in deriving the results should be carefully considered. The error limits in Fig. 5 include four primary sources of uncertainty. In the measured (442) diffracted power $E\omega$ there was a substantial statistical uncertainty because of the extreme weakness of the reflection. This error varied with the number of θ scans made at each temperature. To obtain the integrated intensity $(E\omega/I_0)$, additional error was introduced in the measurement of I_0. Included in the error in I_0 was the uncertainty in the measured (222) diffracted power $E\omega$ and the error in $F(222)$ as reported by Roberto and Batterman.[2] These three errors combined to give the uncertainty in F_{422}. To obtain the electronic contribution in $F(442)$, the anharmonic contribution was computed from neutron measurement. The errors quoted by Keating *et al.*[11] for these measurements were included in the final results for F_{bond}.

In addition to these experimental errors, one further source of uncertainty should be included. In deriving the anharmonic contribution to the (442) reflection from the neutron measurements of the (222) reflection [see Eqs. (5) and (6)], the approximation that the contributions scaled as the product of the Miller indices was used. It is difficult to estimate the accuracy of this approximation without a model for anharmonic vibrations in silicon. The uncertainty in this approximation would be eliminated if neutron measurements of the Si(442) reflection were available. Any conclusion concerning the temperature dependence of $F_{bond}(442)$ must be tempered by the size of these errors.

The temperature dependence of the data in Fig. 5 might be explained by letting $M' = 0$, that is, by

assuming the antisymmetric charge distribution has zero mean-square amplitude of vibration. Neutron and x-ray studies of the Si(222) reflection[2,11] resulted in a curve for $F_{bond}(222)$ which was qualitatively fit by letting $M' = \frac{1}{2}M$, implying that the core and bond electrons have different vibrational amplitudes. These apparent inconsistencies in the two sets of data might be resolved by letting f_a vary with temperature implying that the amount and/or shape of the bonding charge distribution changes with temperature. Phillips has presented thoughts along these lines in a recent publication.[23] The temperature dependence for $f_a(222)$ and $f_a(442)$ would, in general, be different. The above speculation is based on rather marginal experimental evidence. However, the implications are sufficiently interesting to suggest further experiments designed to verify the trends observed in the Si(222) and (442) data.

Our results may be summarized as follows: We have shown the existence of the forbidden (442) reflection in silicon. Anharmonic vibrations cause the reflection's intensity to decrease to zero at about 250 °C and then increase at higher temperatures. Correcting for the anharmonic contribution determined from previous neutron-diffraction measurements, we determined the temperature dependence of the structure factor due to the antisymmetric bond charge. The corrected (442) structure factor appears to be temperature independent. Because of the large experimental errors due to the low intensities involved, we feel further experiments are necessary before definite conclusions can be drawn concerning the bond charge motion.

*Work supported by the Advanced Research Projects Agency through the Materials Science Center at Cornell University.

†Present address: Department of Crystallography, University of Pittsburgh, Pittsburgh, Pa. 15213.

[1]W. H. Bragg, Proc. Phys. Soc. (London) 33, 304 (1921).

[2]J. B. Roberto and B. W. Batterman, Phys. Rev. B 2, 3220 (1970).

[3]R. Colella and A. Merlini, Phys. Status Solidi 18, 157 (1966).

[4]J. J. DeMarco and R. J. Weiss, Phys. Rev. 137, A1869 (1965).

[5]M. Renninger, Z. Krist. 113, 99 (1960).

[6]E. Wolfel *et al.*, Z. Physik. Chem. (Frankfurt) 21, 133 (1959).

[7]B. Dawson, Proc. Roy. Soc. (London) A298, 255 (1967).

[8]B. Dawson, Proc. Roy. Soc. (London) A298, 379 (1967).

[9]B. Borie (private communication).

[10]A. A. Maradudin, *Solid State Physics*, Suppl. 3 (Academic, New York, 1963).

[11]D. Keating, A. Nunes, B. W. Batterman, and J. Hastings, Phys. Rev. B 4, 2472 (1971).

[12]B. W. Batterman, J. Appl. Phys. 28, 1236 (1957).

[13]M. Renninger, Z. Krist. 106, 141 (1937).

[14]H. Cole, F. Chambers, and H. Dunn, Acta Cryst. 15, 138 (1962).

[15]L. D. Jennings (private communication).

[16]B. W. Batterman and D. R. Chipman, Phys. Rev. 127, 690 (1962).

[17]D. T. Cromer and J. T. Waber, Acta Cryst. 18, 104 (1965).

[18]D. T. Cromer and David Liberman, J. Chem. Phys. 53, 1891 (1970).

[19]B. Dawson and P. L. Sanger, Proc. Roy. Soc. (London) A301, 195 (1967).

[20]J. J. DeMarco and R. J. Weiss, Phys. Rev. 137, A1860 (1965).

[21]M. Jaros and P. K. W. Vinsome, J. Phys. C 2, 2373 (1969).

[22]J. C. Phillips, Phys. Rev. 166, 832 (1968).

[23]J. C. Phillips, Phys. Letters 37A, 434 (1971).

PHYSICAL REVIEW B VOLUME 6, NUMBER 10 15 NOVEMBER 1972

Magnetic Surface States in Zinc*

J. P. Rahn and J. J. Sabo, Jr.
Department of Physics, University of Washington, Seattle, Washington 98195

(Received 5 July 1972)

The magnetic fields at which magnetic-surface-state transitions occur were measured as a function of sample orientation in the three principal planes of zinc. These low-field microwave-frequency transitions dominate the surface impedance from 0 to 100 Oe. Three distinct series are presented and these are assigned to regions on the Fermi surface. The anisotropy of these series is compared with predictions of orthogonalized-plane-wave band models. The Fermi velocities on the third-band lens are extracted and presented.

I. INTRODUCTION

Although considerable experimental work[1-3] has been done in recent years to validate the Prange–Nee[4] theory of magnetic surface states, the effect has not been used extensively to obtain parameters at points on the Fermi surface.[5,6] In this paper we report an extensive experimental investigation and